Single-Leg Forward Hopping via Nonlinear Modes

Calzolari, Davide; Della Santina, C.; Giordano, Alessandro Massimo; Albu-Schaffer, Alin

DOI
10.23919/ACC53348.2022.9867538

Publication date
2022

Document Version
Final published version

Published in
Proceedings of the American Control Conference (ACC 2022)

2022 American Control Conference (ACC)
Atlanta, USA, June 8-10, 2022

Single-Leg Forward Hopping via Nonlinear Modes

Davide Calzolari[1], Cosimo Della Santina[1,2], Alessandro M. Giordano[1], Alin Albu-Schäffer[1]

***Abstract*— Implementing dynamic legged locomotion entails stabilizing oscillatory behaviors in complex mechanical systems. Whenever possible, locomotion algorithms should also exploit the improved capabilities of elastic elements added to the structure to improve efficiency and robustness. This work aims to shed some light on implementing generic dynamic locomotion by stabilizing nonlinear modes. The nonlinear modal analysis extends the linear modal theory to nonlinear systems and thus characterizes the oscillations that a robot can execute as autonomous evolutions. We execute forward hopping motions with a single segmented elastic leg as the first step towards generic modal locomotion. We propose a locomotion algorithm that exploits the modes of an extension of the SLIP model. We develop this strategy to generalize to other robotic systems, and we extensively validate it with experiments on an elastically actuated segmented leg.**

I. Introduction

Introducing elasticity into the mechanical structure of robotic systems should allow them to implement efficient oscillatory behavior. Well-known results in linear modal analysis drive this intuition [1, Sec. 2]. Furthermore, vertebrate animals - with their elastic tendons and muscles - provide plenty of examples of using elasticity in periodic tasks [2]. These ideas led to introducing elastic elements to the robot's mechanical structure and thus to the fields of continuum and articulated soft robotics [3]. The question of unraveling the potential of robots built according to these principles has seen increasing attention in the last decade [4].

Among oscillatory tasks, the most relevant is probably locomotion [5], within which exploitation of compliance has been thoroughly investigated [6], [7]. Many of these works focus on the spring-loaded inverted pendulum (SLIP) model [8], [9], for which robotic implementations also exist [10], [11]. Simple reset policies are already sufficient for generating stable gates in the SLIP [12]. More complex strategies, intrinsically robust to terrain uncertainties, have been investigated as well [13], [14]. It is well-known that largely passive locomotion patterns can arise in walkers that are more complex than a SLIP [15]–[17]. However, these systems have never been extended beyond the proof-of-concept to full-fledged robots. Instead, the vastly more popular approach is to match the high dimensional dynamics to the SLIP model via feedback model matching [18]–[21]. This approach effectively deals with highly articulated systems.

This project has received funding from the European Research Council (ERC) under the European Union's Horizon 2020 research and innovation programme (grant agreement No 835284). [1] The authors are with the Department of Informatics, Technical University of Munich (TUM), 85748 Garching, Germany, and with the Institute of Robotics and Mechatronics, German Aerospace Center (DLR), 82234 Weßling, Germany davide.calzolari,Alin.Albu-Schaeffer@dlr.de . [2] Cosimo Della Santina is with the Cognitive Robotics Department, Delft University of Technology (TU Delft), Delft, The Netherlands c.dellasantina@tudelft.nl.

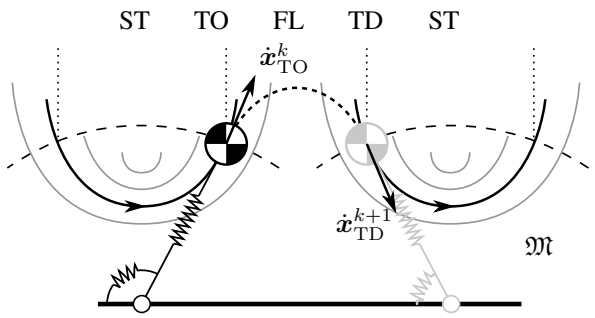

Fig. 1. Connecting nonlinear modes of consecutive stance phases (ST) using geometric properties of the mode and leg control during the flight phase (FL). The touch down and take off transition events are denoted TD and TO, respectively.

However, it relies on model cancellations and therefore only partially exploits the robot's natural dynamics.

In this work, we take an alternative route grounded in control of periodic orbits [22]–[24] that may eventually lead to full exploitation of the natural dynamics of generic elastic-legged systems. In this context, nonlinear modal theory [1], [25] allows to identify families of oscillations that the robot can execute *naturally*. For example, authors of [26] have proven that modal gaits exist embedded in a soft quadruped, but proposed no controller for regulating them. In our recent work, we have proposed feedback controllers that can excite these oscillations - called nonlinear modes - in fixed based robots [27], [28]. The goal is to help the robot expressing its natural capabilities, rather than being forced to perform generic motions. Modal periodic pick-and-place is analyzed in [29], and preliminary execution locomotion patterns in [30]. Both rely on excitation of line-shaped modes. Nonlinear modes are instead used in [31] and [32] to swing and to jump with a single leg, both in place.

In summary, nowadays, no algorithm can leverage fully nonlinear modes to construct locomotion patterns and implement dynamic locomotion. As the first step in this direction, this paper introduces an algorithm for forward-jumping and reports its experimental validation. This preliminary investigation focuses on the p-SLIP, an extension of the SLIP model featuring nonlinear polar and radial springs. Nonetheless, we develop the strategy to be readily generalizable to other articulated-legged systems by using only ingredients that are robot-agnostic.

II. Design Principles using Nonlinear Modes

A. Dynamics of the p-SLIP template

We focus on the template model in Fig. 2, which extends the SLIP model by adding a polar spring. Also, we consider generic nonlinear springs, and a force and a torque acting in parallel to them. We refer to this model as p-SLIP in the

978-1-6654-5196-3/$31.00 ©2022 AACC

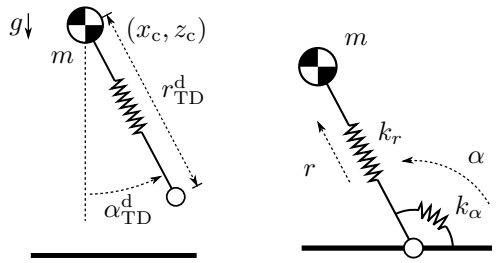

(a) Flight phase (b) Stance Phase

Fig. 2. The two phases in which the p-SLIP can find itself: stance - foot is on the ground; and flight - no ground contact. We assume that the foot is the only possible point of contact.

following. The polar spring may represent the stiffness of the ankle, or it can arise from a constraint on the total rotation of the body. We will show that the latter is embedded on the physical device on which we will perform experiments. The polar spring can also be realized in a quadruped, for example using the two support legs of each diagonal pair during trotting.

The p-SLIP is a hybrid system, with two continuum dynamics models (stance and flight phases) and transition maps. During stance phase, the foot is considered connected to the ground through a revolute joint (no slippage). Standard Lagrangian derivations yield the following stance phase dynamics

$$\begin{aligned} \ddot{\alpha} &= -\frac{2\dot{r}\dot{\alpha}}{r} + \frac{g}{r}\sin\alpha - \frac{k_\alpha(\alpha)}{mr^2} + \frac{\tau_\alpha}{mr^2}\ , \\ \ddot{r} &= r\dot{\alpha}^2 - g\cos\alpha - \frac{k_r(r)}{m} + \frac{\tau_r}{m}\ , \end{aligned} \tag{1}$$

where $(\alpha, r) \in \mathbb{R}^2$ are the polar coordinates of the CoM, $m \in \mathbb{R}^+$ is the total mass, g is the gravitational acceleration, $(k_\alpha, k_r) \in \mathbb{R}^2$ are the potential generalized elastic forces, and $(\tau_\alpha, \tau_r) \in \mathbb{R}^2$ are the generalized actuation forces. We assume that $k_\alpha(\alpha) = -k_\alpha(-\alpha)$, which is generally non-restrictive for elastic actuated legged system. For the rest of the paper, let r_0 denote the rest length of the radial spring, i.e., $k_r(r_0) = 0$, and α_0 the rest angle of the polar spring, i.e., $k_\alpha(\alpha_0) = 0$.

When in flight, the body follows a ballistic dynamics

$$\ddot{x}_c = 0, \quad \ddot{z}_c = -g, \quad \alpha = \alpha^d_{TD}, \quad r = r^d_{TD}\ , \tag{2}$$

where x_c and z_c are the horizontal and vertical Cartesian configurations of the trunk CoM, respectively. As usual in works about SLIP models, we assume that the angle of attack α can be controlled during the flight phase. This is interpreted as the leg inertia being negligible compared to the main body. Thus, the inputs of system (2) are α^d_{TD} and r^d_{TD}, which are the desired angle of attack and leg extension.

The transition and guard conditions maps are reported in Fig. 3, where $F_z \in \mathbb{R}$ is the vertical component of the force generated by the springs while pushing into the ground, and $\boldsymbol{J}_c(\alpha, r) \in \mathbb{R}^{2\times 2}$ is the Jacobian associated with the Cartesian change of coordinates, i.e., $(\dot{x}_c,\ \dot{z}_c) = \boldsymbol{J}_c(\alpha, r)(\dot{\alpha},\ \dot{r})$. At touchdown, the CoM velocity $\dot{\boldsymbol{x}}_{c,TD}$ determines $(\dot{\alpha}, \dot{r})_{TD}$, while the initial velocity of the CoM ballistic trajectory is determined at the moment of take off.

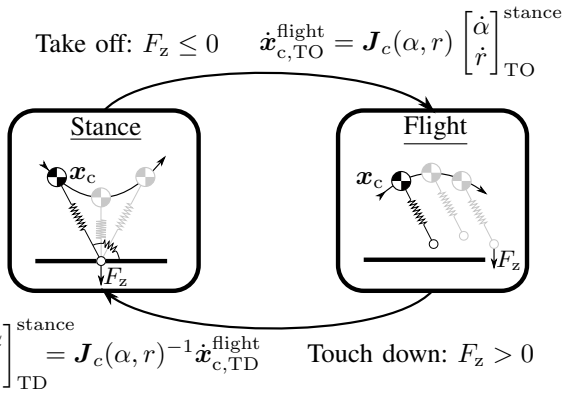

Fig. 3. The full hybrid dynamics, with transition guards and maps reported. The TO and TD subscripts denote the velocities at take off and touch down, respectively.

B. The nonlinear modes of the extended SLIP

We use nonlinear modal analysis to characterize the family of natural oscillations that the p-SLIP[1] can perform as autonomous evolutions while in the stance phase. We focus here on the stance phase only because the theory is still restricted to non-hybrid systems. In the following subsection, we will show how this information can be used in the hybrid regime.

Within nonlinear modal theory [1], the flat invariant collections of regular oscillations that we find in linear systems (eigenspaces) are curved into 2-dimensional *invariant* submanifolds embedded in the robot's state space (eigenmanifolds). Still, these objects collect infinite self-similar and hyper-efficient periodic orbits - one for each energy level. An eigenmanifold $\mathfrak{M}$ of the p-SLIP can be represented as follows

$$\begin{aligned} \mathfrak{M} \simeq \big\{ &(\alpha, r, \dot{\alpha}, \dot{r}) \in \mathbb{R}^4 \mid \exists (x_m, \dot{x}_m) \in \mathbb{R}^2 \\ &\text{s.t. } (\alpha, r) = X(x_m, \dot{x}_m),\ (\dot{\alpha}, \dot{r}) = \dot{X}(x_m, \dot{x}_m) \big\}, \end{aligned} \tag{3}$$

where $(X, \dot{X}) : \mathbb{R}^2 \to \mathbb{R}^2 \times \mathbb{R}^2$ is a polynomial approximation of the coordinate expressions of the natural embedding of $\mathfrak{M}$ into $\mathbb{R}^4$. The first argument of $(X, \dot{X})$ is called *master* variable x_m. Usually, when evaluating $X, \dot{X}$ a retraction is implicitly defined from (α, r) to x_m. These two functions encode all the necessary information about the eigenmanifold geometry, and as such they play an important role in our control framework. Solving in the Galerkin sense the tangency constraints discussed in [27], yields a suitable approximation of the embedding.

The p-SLIP has at least two eigenmanifolds, tangent to eigenspaces of the linearized system. One is the eigenmanifold collecting *hopping in place* motions. In this special case the tangency constraints can be solved without any approximation, and the result is the following line-shaped manifold

$$\{(\alpha, r, \dot{\alpha}, \dot{r}) \in \mathbb{R}^4 \mid \alpha \equiv 0,\ \dot{\alpha} \equiv 0\}.$$

These are vertical oscillations in the r direction, governed by the modal dynamics $\ddot{r} = -g + k_r(r)/m$. This can be used to

[1]For the sake of space, we are presenting here the theory specialized to p-SLIP. The interested reader is referred to [1] for more details on the general case.

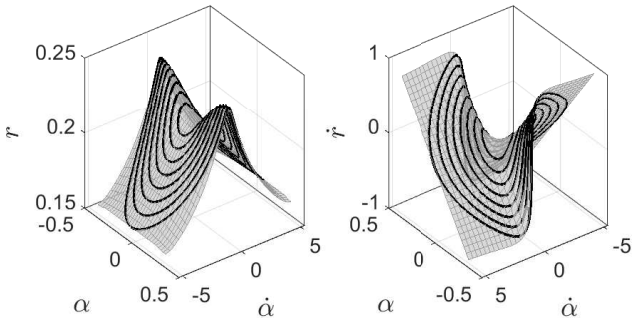

Fig. 4. The manifold depicted in light gray is a polynomial approximation of the Eigenmanifold associated with the mechanical system shown in Figure 2(b), using the parameters discussed in the experimental section. Trajectories on the modes with constant energy levels are displayed with solid black lines. The figure shows the very clear nonlinear character of the Eigenmanifold - in comparison, a linear mode would result in a planar shape.

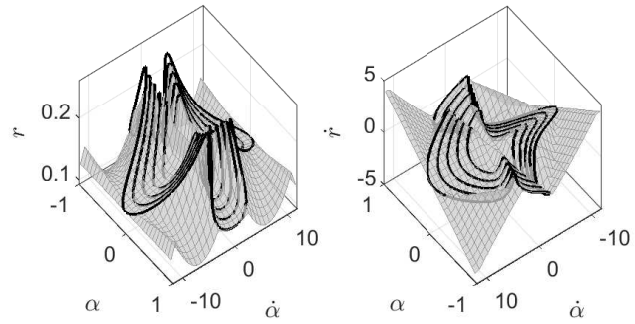

Fig. 5. Another Eigenmanifold of the p-SLIP obtained for the system parameters considered in the simulation section, which are different with respect to the ones for Fig 4. Trajectories on the modes with constant energy levels are displayed with solid black lines.

implement in place hopping, but no forward motion, since no swinging of the main body is involved. As such, we are not concerned with this manifold in this work.

The other eigenmanifold is associated to swing motions, and therefore especially useful for locomotion. In this case a natural choice for the master variable x_m is α. Thus, the first elements of X and $\dot{X}$ are the identity. As examples, we report in Fig. 4 the swing motion manifold for the choice of springs discussed in the experimental section, and in Fig. 5 the manifold for the set of system parameters presented in the simulation section. Examples of autonomous orbits for different energy levels are also reported. Each one corresponds to a swing motion of the p-SLIP with different amplitude. Additionally, Fig. 6 depicts the swinging CoM trajectories in Cartesian coordinates corresponding to orbits on the Eigenmanifold in Fig. 4.

C. Gait Planning Based on Nonlinear Modes

In this work we focus exclusively on the mode related to the stance phase, i.e., we exploit the natural oscillations of the system when the foot is in contact. Let us define the touch down (TD) and take off (TO) related quantities belonging to k-th cycle with the superscript $(\cdot)^{\mathrm{k}}$. In order to benefit from the efficiency of the modes, at each touch down the system should be on the mode. To assure that this is the case, we

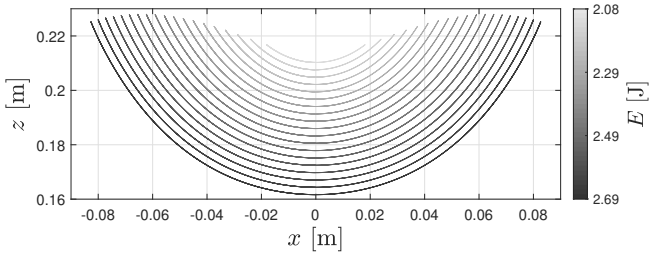

Fig. 6. Trajectories of the CoM in Cartesian coordinates corresponding to autonomous orbits on the Eigenmanifold presented in Fig. 4 for a range of energy levels. In this work, the resulting swinging motion is exploited to build efficient locomotion patterns.

introduce the following matching conditions

$$\begin{bmatrix}\alpha^{\mathrm{k}}_{\mathrm{TD}}\\ r^{\mathrm{k}}_{\mathrm{TD}}\end{bmatrix} \equiv X(\alpha^{\mathrm{k}}_{\mathrm{TD}}, \dot{\alpha}^{\mathrm{k}}_{\mathrm{TD}}) \ , \quad \begin{bmatrix}\dot{\alpha}^{\mathrm{k}}_{\mathrm{TD}}\\ \dot{r}^{\mathrm{k}}_{\mathrm{TD}}\end{bmatrix} \equiv \dot{X}(\alpha^{\mathrm{k}}_{\mathrm{TD}}, \dot{\alpha}^{\mathrm{k}}_{\mathrm{TD}}) \ . \tag{4}$$

Note that the master variable is $x_{\mathrm{m}} = \alpha$, as described in Section II-B. In this manner, the trajectories stay on the mode during stance without the need of corrections.

In order to fulfill condition (4), each k-th stance phase mode must be connected in a proper way to the next $k+1$ stance phase. Figure 1 presents the idea utilized in this paper to perform this connection. Essentially, the take off and touch down events are designed such that fulfilling (4) becomes feasible by properly regulating the angle of attack and leg extension during the flight phase. Note that the uncontrolled ballistic CoM trajectory is determined by $\dot{\alpha}_{\mathrm{TO}}$ and $\dot{r}_{\mathrm{TO}}$, which, in turn, determines $\dot{\alpha}_{\mathrm{TD}}$ and $\dot{r}_{\mathrm{TD}}$.

1) Leg Extension Planning: Let us consider a trajectory on the chosen mode for the stance phase of the p-SLIP, i.e., satisfying (3), and where the TD and TO events occur for the same leg length r, i.e. $r^{\mathrm{k}}_{\mathrm{TD}} = r^{\mathrm{k}}_{\mathrm{TO}}$, then we have the following properties

$$\alpha^{\mathrm{k}}_{\mathrm{TO}} = -\alpha^{\mathrm{k}}_{\mathrm{TD}}, \quad \dot{\alpha}^{\mathrm{k}}_{\mathrm{TO}} = \dot{\alpha}^{\mathrm{k}}_{\mathrm{TD}}, \quad \dot{r}^{\mathrm{k}}_{\mathrm{TO}} = -\dot{r}^{\mathrm{k}}_{\mathrm{TD}}, \tag{5}$$

Furthermore, expressing (5) in Cartesian coordinates allows to also conclude

$$\dot{x}^{\mathrm{k}}_{\mathrm{c,TO}} = \dot{x}^{\mathrm{k}}_{\mathrm{c,TD}} \ , \quad \dot{z}^{\mathrm{k}}_{\mathrm{c,TO}} = -\dot{z}^{\mathrm{k}}_{\mathrm{c,TD}} \ . \tag{6}$$

If the $k+1$ stance phase occurs after a time interval $2\dot{z}^{\mathrm{k}}_{\mathrm{TO}}/g$ with

$$\alpha^{\mathrm{k+1}}_{\mathrm{TD}} = -\alpha^{\mathrm{k}}_{\mathrm{TO}}, \quad r^{\mathrm{k+1}}_{\mathrm{TD}} = r^{\mathrm{k}}_{\mathrm{TO}} \ , \tag{7}$$

then simple ballistic calculations allow to conclude that

$$\dot{x}^{\mathrm{k+1}}_{\mathrm{c,TD}} = \dot{x}^{\mathrm{k}}_{\mathrm{c,TO}}, \quad \dot{z}^{\mathrm{k+1}}_{\mathrm{c,TD}} = -\dot{z}^{\mathrm{k}}_{\mathrm{c,TO}} \ . \tag{8}$$

Thus, by using the transition maps in Fig. 3, (8) and (6)

$$\begin{bmatrix}\dot{\alpha}\\ \dot{r}\end{bmatrix}^{\mathrm{k+1}}_{\mathrm{TD}} = {\boldsymbol{J}_{\mathrm{c}}}^{-1}\begin{bmatrix}\dot{x}_{\mathrm{c}}\\ \dot{z}_{\mathrm{c}}\end{bmatrix}^{\mathrm{k+1}}_{\mathrm{TD}} = {\boldsymbol{J}_{\mathrm{c}}}^{-1}\begin{bmatrix}\dot{x}_{\mathrm{c}}\\ -\dot{z}_{\mathrm{c}}\end{bmatrix}^{\mathrm{k}}_{\mathrm{TO}} = {\boldsymbol{J}_{\mathrm{c}}}^{-1}\begin{bmatrix}\dot{x}_{\mathrm{c}}\\ \dot{z}_{\mathrm{c}}\end{bmatrix}^{\mathrm{k}}_{\mathrm{TD}} = \begin{bmatrix}\dot{\alpha}\\ \dot{r}\end{bmatrix}^{\mathrm{k}}_{\mathrm{TD}} \tag{9}$$

Therefore, at each touch down, the system starts again on the mode. During the flight phase, the control system should guarantee (7), i.e., regulation of the attack angle and leg extension to the desired values.

The desired take off and touch down are designed to occur when $r = r_0$, as shown in Figure 7. This specific design choice avoids requiring a preload for the radial spring at the moment of impact, i.e., the touch down occurs when the spring is at its rest length.

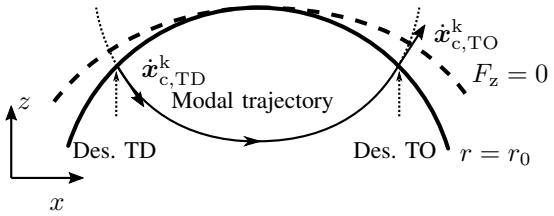

Fig. 7. In order to properly connect the k-th stance phase mode to the mode $k+1$, the conditions $r \leq r_0$ and $r > r_0$ are used to determine whether the system enters the stance or flight phases. The take off is triggered by control instead of waiting for the condition $F_{\mathrm{z}} \leq 0$ to occur.

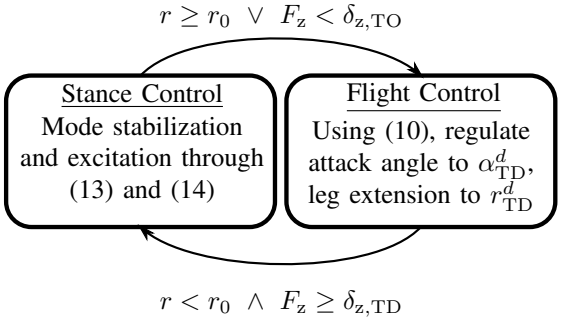

Fig. 8. A state machine manages the switching between the two controllers. The additional conditions on F_{z} are introduced to robustify the switches in practical applications.

2) Attack Angle Planning: Given the modal manifold $\mathfrak{M}$, and a desired energy level E^{d} (related to a desired forward speed), the reference attack angle can be calculated using the intersection of the modal trajectory with the desired leg extension $r^{\mathrm{d}}_{\mathrm{TD}} = r_0$. The required state at touchdown is then

$$\boldsymbol{x}^{\mathrm{d}}_{\mathrm{TD}} = \mathfrak{M}_{E(\boldsymbol{x},\dot{\boldsymbol{x}})=E^{\mathrm{d}}} \cap \{r = r_0, \dot{r} < 0, \mathrm{sign}(\alpha) = s_\alpha\} \ , \tag{10}$$

where $\mathfrak{M}_{E(\boldsymbol{x},\dot{\boldsymbol{x}})=E^{\mathrm{d}}}$ identifies the unique system trajectory on the mode with the energy level E^{d}, and $s_\alpha \in \{-1, 1\}$ is used to pick the desired direction of horizontal motion. We approximate the solution of (10) for $\alpha^{\mathrm{d}}_{\mathrm{TD}}$ analytically, using a polynomial. During the flight phase, the leg is regulated to the desired attack angle $\alpha^{\mathrm{d}}_{\mathrm{TD}}$ and radial length $r^{\mathrm{d}}_{\mathrm{TD}}$. In a real system, this can be achieved by transforming the desired configuration into joint positions, and then directly feeding these to the motors using a position controller.

III. Control Architecture

The control architecture consists of two controllers - one active during stance (foot on the ground) and the other during flight (foot in the air) - which are scheduled by a simple state machine (Fig. 8). The stance controller is designed so to stabilize the swing-like nonlinear mode. The flight controller is used to close the hybrid orbit by regulating the angle of attack and radial length.

A. Phase Detection

The transition in the finite state machine in Fig. 8 corresponds to detection of transitions between the stance and the flying phase, and viceversa. In theory, these guarding conditions can be implemented by directly measuring contact forces through a sensor placed in the foot. This is however not always desirable - e.g., these sensors are expensive and fragile. As an alternative, contact forces can be inferred by comparing the leg extension r with r_0, and using thresholds on the projection of $k_\alpha(\alpha)$ and $k_{\mathrm{r}}(r)$ along the vertical direction with respect to the ground, i.e., F_{z}. Whenever $r < r_0$ and F_{z} is higher than a threshold $\delta_{z,TD}$ for a minimum time interval, the state machine triggers the touch down (TD) event, and the control system reacts to this event. Like-wise, when $r \geq r_0$ or F_{z} is below a threshold $\delta_{z,TO}$, the take-off (TO) event is triggered.

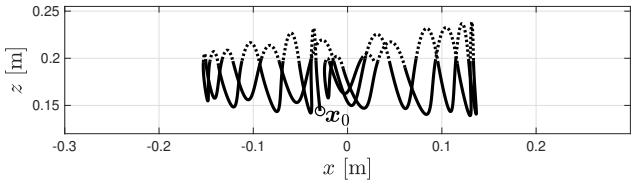

Fig. 9. Non-regular behaviour of the uncontrolled p-SLIP. The system is initialized with $\alpha(0) = 0.2\,\mathrm{rad}$, $r(0) = 0.144\,\mathrm{m}$, $\dot{\alpha}(0) = \dot{r}(0) = 0$, and a constant attack angle $= 0.2\,\mathrm{rad}$. The trajectory of the CoM is depicted with solid lines during stance and with dotted lines during flight.

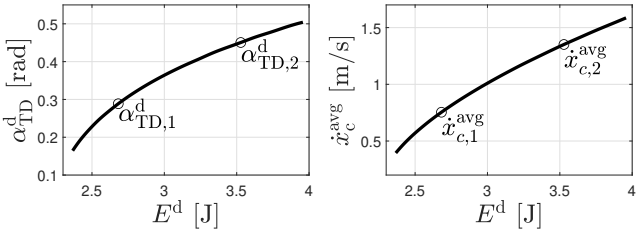

Fig. 10. Left plot: attack angle as function of the mechanical energy using modal information. In order to connect the stance phase modes for different speeds (different energy levels), a proper attack angle is required. The values of the two attack angles corresponding to a low and a high energy level used for the simulations are marked with circles. Right plot: average forward speed for different energy levels.

B. Stance Phase Mode Controller

The overall action of the mode controller is defined as [27]

$$\boldsymbol{\tau}_{\mathrm{ctrl}}(\boldsymbol{x}, \dot{\boldsymbol{x}}) = \boldsymbol{\tau}_{\mathrm{s}}(\boldsymbol{x}, \dot{\boldsymbol{x}}) + \boldsymbol{\tau}_{\mathrm{in}}(\boldsymbol{x}, \dot{\boldsymbol{x}}; E^{\mathrm{d}}), \tag{11}$$

where $(\boldsymbol{x}, \dot{\boldsymbol{x}})$ is the system state, and

$$\begin{aligned} \boldsymbol{\tau}_{\mathrm{s}} &= k\boldsymbol{M}_x(\boldsymbol{x}) \left(\boldsymbol{x} - X(x_{\mathrm{m}}, \dot{x}_{\mathrm{m}}) + \frac{d}{k}(\dot{\boldsymbol{x}} - \dot{X}(x_{\mathrm{m}}, \dot{x}_{\mathrm{m}})) \right) \ , \\ \boldsymbol{\tau}_{\mathrm{in}} &= \gamma \boldsymbol{M}_x(\boldsymbol{x}) \dot{\boldsymbol{x}} (E^{\mathrm{d}} - E(\boldsymbol{x}, \dot{\boldsymbol{x}})) \ , \end{aligned} \tag{12}$$

with $k > 0, d > 0$ being the proportional and derivative gains respectively, $\gamma > 0$ the energy regulation gain, and $\boldsymbol{M}_x$ is the inertia matrix in $\boldsymbol{x}$ coordinates. The goal of $\boldsymbol{\tau}_{\mathrm{s}}$ is to stabilize the swing eigenmanifold, i.e., $(\boldsymbol{x}, \dot{\boldsymbol{x}}) \to (X, \dot{X})$. The role of $\boldsymbol{\tau}_{\mathrm{in}}$ is to select the right amplitude of oscillation by regulating the energy level - i.e., $E \to E^{\mathrm{d}}$. This way, a single swing-like modal orbit can be stabilized without relying on trajectory tracking controllers. Note that the overall controller is designed such that $\boldsymbol{\tau}_{\mathrm{ctrl}} \to 0$ (hyper-efficient oscillation) when the system converges to the desired modal trajectory. This is possible because the modes are natural evolutions of the system dynamics. More details about this strategy can be found in [28]. As mentioned in Section II-B, in the case of the template model considered in this work, $\boldsymbol{\tau}_{\mathrm{ctrl}} = (\tau_\alpha, \tau_{\mathrm{r}})$,

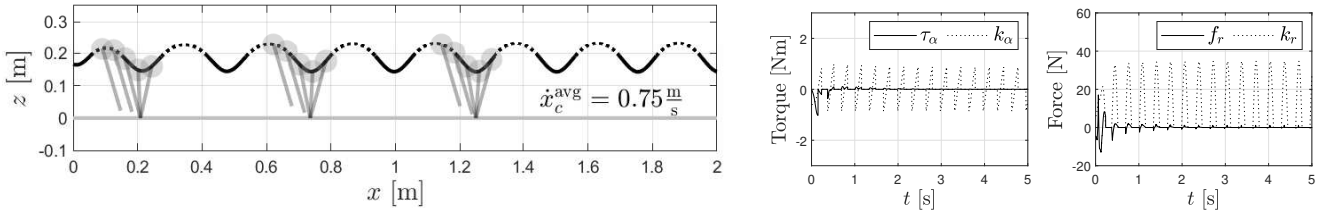

(a) Low desired energy level

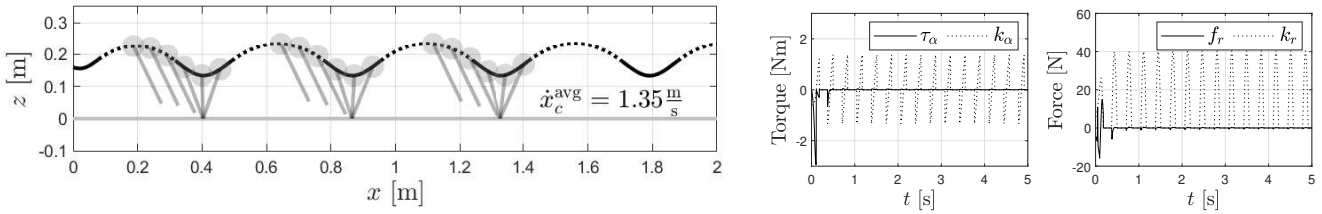

(b) High desired energy level

Fig. 11. Simulations of the p-SLIP controlled using the proposed approach showing stable forward hopping for two energy levels. For both simulations, the system is initialized with $\alpha(0) = 0.2\,\text{rad}$, $r(0) = 0.19\,\text{m}$, $\dot{\alpha}(0) = \dot{r}(0) = 0$. Control inputs for each simulation are also reported, together with the corresponding spring contributions. After few steps, the motion evolves along the nonlinear mode, and the control action converges to zero.

$\boldsymbol{M}_x \in \mathbb{R}^{2\times 2}$ is a diagonal matrix with elements mr^2 and m, and we take $x_m = \alpha$. Thus, in our case, (12) becomes

$$\begin{aligned} \frac{\tau_\alpha}{m} &= \gamma(E^{\text{d}} - E(\alpha, r, \dot{\alpha}, \dot{r}))r^2\dot{\alpha}\,, \\ \frac{\tau_{\text{r}}}{m} &= \gamma(E^{\text{d}} - E(\alpha, r, \dot{\alpha}, \dot{r}))\dot{r} + k(r - X_{\text{r}}(\alpha, \dot{\alpha})) + d(\dot{r} - \dot{X}_{\text{r}}(\alpha, \dot{\alpha}))\,. \end{aligned} \tag{13}$$

This controller may generate forces that violate the unilateral ground constraint (i.e., attempting to pull the foot away from the floor) and thus degrade the excitation of the oscillation. Therefore, the control action is saturated as

$$\begin{aligned} \tau_\alpha^{\text{sat}} &= \begin{cases} \min(\tau_\alpha,\ -\delta_\alpha k_\alpha(\alpha)), & \text{if } \alpha \geq 0 \\ \max(-\delta_\alpha k_\alpha(\alpha),\ \tau_\alpha), & \text{otherwise,} \end{cases} \\ \tau_{\text{r}}^{\text{sat}} &= \max(-\delta_{\text{r}} k_{\text{r}}(r),\ \tau_{\text{r}}), \end{aligned} \tag{14}$$

to guarantee $F_{\text{z}} > 0$, where $\delta_\alpha, \delta_{\text{r}} \in [0, 1]$ are used to tune a safety margin.

C. Example in Simulation

We carry out simulations for a simple implementation of the p-SLIP in order to demonstrate that stable forward hopping can be achieved with the proposed control architecture. A model with the following parameters is considered: $m = 1\,\text{kg}$, $k_\alpha(\alpha) = k_1\alpha$ with $k_1 = 3\,\text{Nm/rad}$, $k_{\text{r}}(r) = k_2 r$ with $k_2 = 600\,\text{N/m}$, and $r_0 = 0.20\,\text{m}$.

In order to highlight the irregular motion that generally arises from the the hybrid dynamics of the p-SLIP, the system is simulated with an initial condition not on the mode and holding a constant angle of attack during the aerial phase. The resulting trajectories of the CoM in Cartesian coordinates are presented in Fig. 9.

In a further simulation, the proposed control strategy is used to perform hopping at two different energy levels. Figure 5 presents the Eigenmanifold of the mechanical system associated with the swing motion. Following the planning strategy described in Section II-C, the desired attack angles are determined using the relationship with the desired energy provided by the mode. Figure 10 presents the polynomial approximation of $\alpha_{\text{TD}}^{\text{d}}$ as function of E^{d} within the studied energy range. The CoM trajectories resulting from the simulations are depicted in Fig. 11, together with snapshots of the system. The simulations show that regular and modal motion is achieved with the proposed controller, using exclusively the natural exchange of kinetic and potential energy since $\boldsymbol{\tau}_{\text{ctrl}} = 0$ on the mode as shown in the plots of the control inputs in Fig. 11.

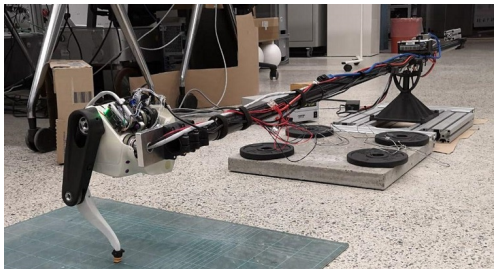

Fig. 12. Experimental setup used to validate the strategy proposed in this paper. An elastically actuated articulated leg is connected to a pole hinged at a point. The pole constraints the rotation of the trunk body, thereby forcing the system to evolve along the sagittal plane with free translation and fixed rotation of the trunk.

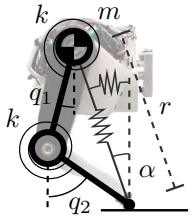

TABLE I
SYSTEM PARAMETERS

Trunk body	m	822	gr
Hip Link	-	122	gr
Shank Link	-	6	gr
Link Length	l	12	cm
Springs	k	2.9	$\frac{\text{Nm}}{\text{rad}}$

Fig. 13. BERT 2-DoF leg. Serial elastic actuators with soft springs drive each link. The links are lightweight: most of the mass is due to the actuators and the support hook. The analogous p-SLIP model is also reported.

IV. Implementation and Experiments

We perform experiments with the latest iteration of the elastic leg proposed in [30], which is a 2-DoF segmented leg, actuated through series elastic actuators. Fig. 13 shows a

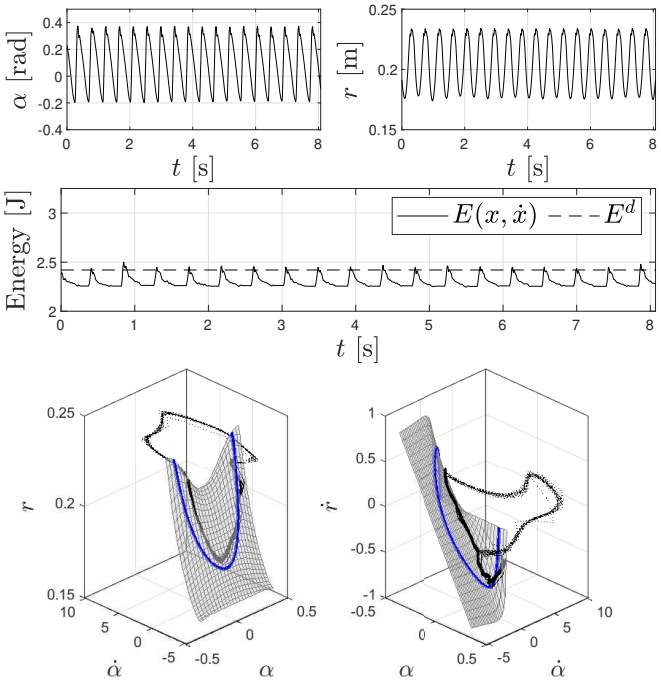

Fig. 14. Experiment 1a. Top plots: trajectories of the system in the coordinates defined in (19). Center plots: mechanical energy during the stance phases (a constant signal is hold during flight). Bottom plots: trajectories of the system in state space using the presented mode controller for $E^{\mathrm{d}} = 2.42J$. Both stance phase trajectories (solid black lines) and flight phase trajectories (dotted black lines) are depicted. Only the useful slice of the mode is shown (depending on the hopping direction).

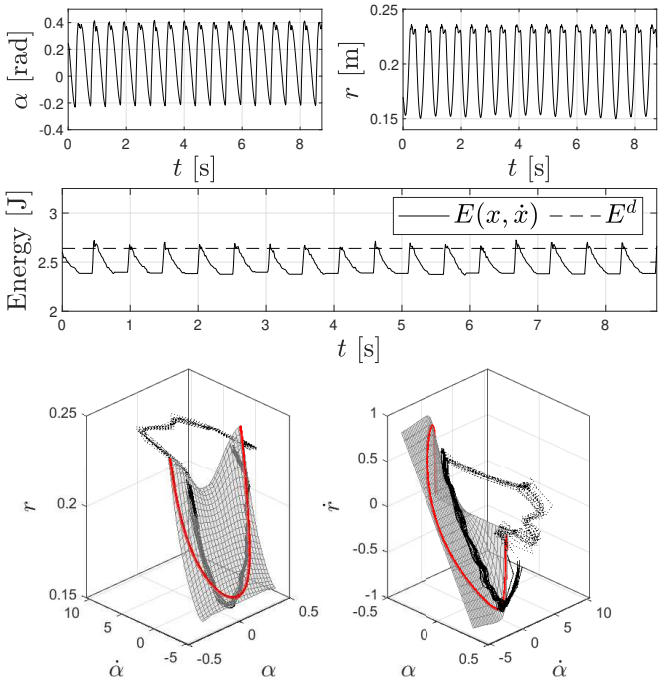

Fig. 15. Experiment 1b. Top plots: trajectories of the system in the coordinates defined in (19). Center plots: mechanical energy during the stance phases. Bottom plots: trajectories of the system in state space using the presented mode controller for $E^{\mathrm{d}} = 2.64J$.

side-view of this leg, with its kinematic model superimposed. Tab. I reports the physical parameters as directly measured from the system. Fig. 12 shows the whole setup, composed of a pole rigidly connected to the hopping robot and hinged at a point; in the setup, the rotation of the main body is thus fixed. The dynamics is described by the equations

$$\boldsymbol{M}(\boldsymbol{q})\ddot{\boldsymbol{q}} + \boldsymbol{C}(\boldsymbol{q},\dot{\boldsymbol{q}})\dot{\boldsymbol{q}} + \boldsymbol{g}(\boldsymbol{q}) + k(\boldsymbol{q}-\boldsymbol{\theta}) = \boldsymbol{J}_{\mathrm{f}}^{\mathrm{T}}\boldsymbol{\lambda}\,, \quad (15)$$

$$\boldsymbol{B}\ddot{\boldsymbol{\theta}} + k(\boldsymbol{\theta}-\boldsymbol{q}) = \boldsymbol{\tau}_m\,. \quad (16)$$

where $\boldsymbol{q} = (q_1, q_2) \in \mathbb{R}^2$ are the joint angles defined as in Fig. 13, $\boldsymbol{\theta} = (\theta_1, \theta_2) \in \mathbb{R}^2$ are the motor angles, $k \in \mathbb{R}$ is the stiffness of both springs, $\boldsymbol{J}_{\mathrm{f}} \in \mathbb{R}^{2\times 2}$ is the foot Jacobian, $\boldsymbol{\lambda} \in \mathbb{R}^2$ are the ground reaction forces, and the other terms are defined as usual. The vertical force F_{z} is reconstructed using the measured spring deflections. In our case, this estimation is accurate because the leg mass and joint friction are very low.

A. Low Level Controller

We control the motors' angles $\boldsymbol{\theta}$ using a PID strategy

$$\boldsymbol{\tau}_m = -K_{\mathrm{p}}(\boldsymbol{\theta}-\boldsymbol{\theta}^{\mathrm{ref}}) - K_{\mathrm{d}}\dot{\boldsymbol{\theta}} - K_{\mathrm{i}}\int(\boldsymbol{\theta}-\boldsymbol{\theta}^{\mathrm{ref}})\mathrm{d}t, \quad (17)$$

where $\boldsymbol{\theta}^{\mathrm{ref}}$ is the reference motor position, and $K_{\mathrm{p}}, K_{\mathrm{i}}, K_{\mathrm{d}} \in \mathbb{R}$ are three positive gains. In practice, motor angles $\boldsymbol{\theta}$ have much faster dynamics than joint angles $\boldsymbol{q}$, thus we assume $\boldsymbol{\theta} \simeq \boldsymbol{\theta}^{\mathrm{ref}}$. Under this assumption the leg behaves as the 2-DoF system $\boldsymbol{M}(\boldsymbol{q})\ddot{\boldsymbol{q}}+\boldsymbol{C}(\boldsymbol{q},\dot{\boldsymbol{q}})\dot{\boldsymbol{q}}+\boldsymbol{g}(\boldsymbol{q})+k(\boldsymbol{q}-\boldsymbol{\theta}^{\mathrm{ref}})-\boldsymbol{J}_{\mathrm{f}}^{\mathrm{T}}\boldsymbol{\lambda} \simeq \boldsymbol{0}$. We then select the reference position $\boldsymbol{\theta}^{\mathrm{ref}}$ as

$$\boldsymbol{\theta}^{\mathrm{ref}} = \frac{\boldsymbol{\tau}_{\mathrm{ctrl}}^{\mathrm{q}}}{k} + \boldsymbol{q}_0 \quad (18)$$

where $\boldsymbol{q}_0 \in \mathbb{R}^2$ is a virtual setpoint and $\boldsymbol{\tau}_{\mathrm{ctrl}}^{\mathrm{q}} \in \mathbb{R}^2$ an equivalent torque applied at joint level. This results in the following parallel elastically actuated system $\boldsymbol{M}(\boldsymbol{q})\ddot{\boldsymbol{q}} + \boldsymbol{C}(\boldsymbol{q},\dot{\boldsymbol{q}})\dot{\boldsymbol{q}} + \boldsymbol{g}(\boldsymbol{q}) + k(\boldsymbol{q}-\boldsymbol{q}_0) - \boldsymbol{J}_{\mathrm{f}}^{\mathrm{T}}\boldsymbol{\lambda} \simeq \boldsymbol{\tau}_{\mathrm{ctrl}}^{\mathrm{q}}$.

B. Change of coordinates: from segmented leg to p-SLIP

Motivated by Tab. I, we consider the mass and inertia of the links negligible compared to the trunk. As suggested in [30], we introduce the change of coordinates

$$\alpha = (q_1+q_2)/2, \quad r = l\sqrt{2(1+\cos(q_2-q_1))}. \quad (19)$$

The dynamics of the system written in (α, r)-coordinates is the p-SLIP in stance phase (1), when naming the generalized forces as

$$\boldsymbol{\tau}_{\mathrm{ctrl}} = (\tau_\alpha, \tau_{\mathrm{r}}), \quad (20)$$

and taking the elastic potential forces equal to

$$k_\alpha(\alpha) = -2k(\alpha-\alpha_0),\ k_{\mathrm{r}}(r) = -\frac{k}{\sqrt{(4l^2-r^2)}}(\rho(r)-\rho(r_0)), \quad (21)$$

where $\rho(r) = \arccos\left(\frac{1-r^2}{2l^2}\right)$. The rest attack angle and rest length are referred α_0 and r_0 respectively, and are related to $\boldsymbol{q}_0$ through (19). Note that coherently with the general template, α and r represent here the polar coordinates of the leg's CoM, which is coincident with the trunk's COM, situated at the hip joint.

We have shown this way that under assumption of negligible hip and shank mass and inertias, the dynamics of our leg during stance phase is equivalent to the one of the p-SLIP. It is immediate to see that same steps also results in a same flight phase dynamics (2). Therefore, our experimental device is equivalent to a p-SLIP, and therefore we can apply the algorithms discussed above to this system without

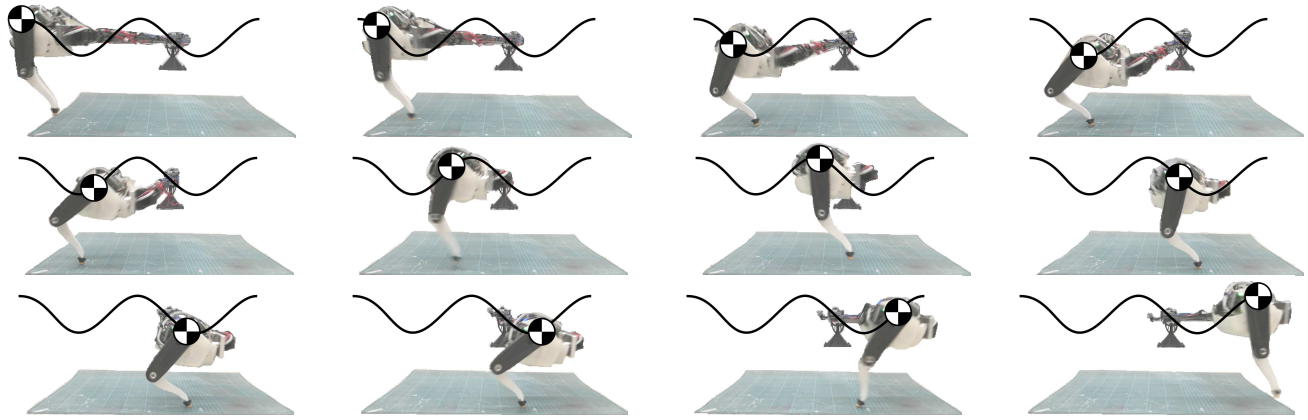

Fig. 16. Experiment 1b: snapshots of the leg performing forward hopping on the mode. The stills allow to appreciate the compression and decompression phases of the leg. The kinetic energy of the main body and the energy stored in the springs are exploited to perform the swing during the stance phase.

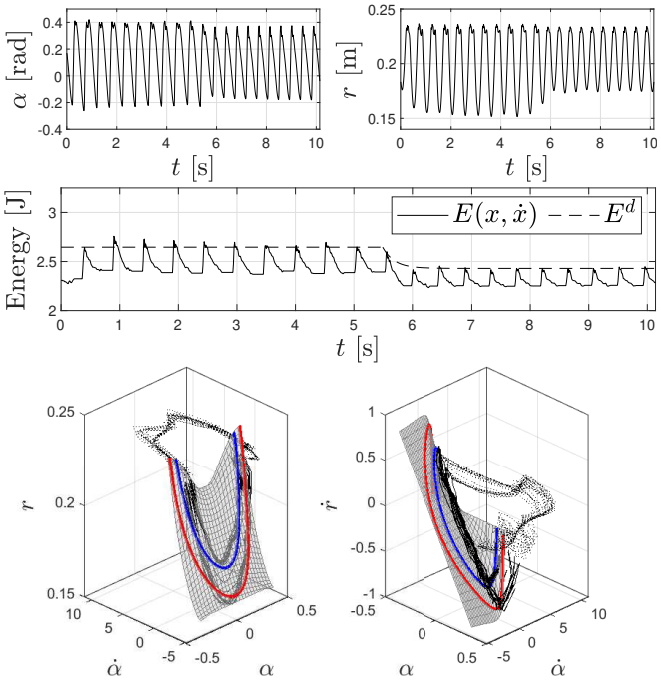

Fig. 17. Experiment 2. The desired energy level is decreased from an high value to a lower value during the hopping. The experiment shows that the system can regulate its forward velocity in controlled and stable way.

the need of any feedback matching. For the spring rest configuration $q_1 = -q_2 = 17\,\mathrm{deg}$ chosen for the experiments (corresponding to $r_0 = 0.2295\,\mathrm{m}$), the swing eigenmanifold of the system is shown in Fig. 4.

Finally, in view of (18), we transform the input forces in (20) to joint space as follows

$$\boldsymbol{\tau}^{\mathrm{q}}_{\mathrm{ctrl}} = \boldsymbol{J}^{\mathrm{T}}_{\alpha,\mathrm{r}}(\boldsymbol{q})\boldsymbol{\tau}_{\mathrm{ctrl}}\,, \tag{22}$$

where $\boldsymbol{J}_{\alpha,\mathrm{r}}(\boldsymbol{q}) \in \mathbb{R}^{2\times 2}$ is the Jacobian associated with the change of coordinates in (19), i.e., $(\dot{\alpha},\, \dot{r}) = \boldsymbol{J}_{\alpha,\mathrm{r}}(\boldsymbol{q})\dot{\boldsymbol{q}}$.

C. Experiment 1: hopping forward with constant energy

The controller presented in Sec. III and depicted in Fig. 8 is implemented to perform stable forward hopping with the experimental leg. During the stance phase, controller (13) is used with gains $\gamma = 20, k = 30$, and $d = 10$. Two different energy levels are tested: a "slow" target energy $E^{\mathrm{d}} = 2.42J$, and a "fast" target $E^{\mathrm{d}} = 2.64J$, corresponding to a relatively faster gait. The desired angles of attack are retrieved using the relationship with the desired energy. The results of the two experiments are presented in Fig. 14 and Fig. 15, which depict the evolution of system trajectories in time and in state space for both stance and flight phase, together with the evolution of the mechanical energy for each experiment. The trajectories on the mode associated with the "slow" and "fast" target energies are shown in solid blue and red, respectively. Additionally, snapshots of the hopping motion are shown in Fig. 16. The system is dropped from approximately 5 cm above ground, and stable regular motion is achieved after a brief transient. Both experiments show that the motion during the stance phase occurs along the Eigenmanifold (or very close to it), and that enough energy is injected at each phase to sustain the designed locomotion cycle. A few mid-air oscillations of the leg can be detected: this happens during the flight phase, since both the leg inertia and damping in the joints are very low, and accurate joint control is hard to obtain. This can reduce the precision of the effective angle of attack with which the robot impacts the ground. Nevertheless, the trajectories mainly evolve on the mode, hence the results demonstrate that natural oscillations of the mechanical system are being exploited to realize the dynamic gait. Notice that this is achieved regardless of the assumptions made for the generation of the nonlinear mode, the parametric uncertainties, and the lack of other feedback actions (like template-matching), which highlights, to some extent, the intrinsic robustness of the presented approach.

D. Experiment 2: switching energy level

The convergence properties and robustness of the mode controller are tested in a second experiment by switching energy levels during operation. The same "slow" and "fast" target energy values from the previous experiment are considered. The results are reported in Fig. 17. First, the high value is commanded, and the system, starting from outside the mode, accelerates during each stance phase in order to oscillate at this energy. As soon as the desired orbit is reached, the lower energy value is commanded. The robot

decelerates accordingly and converges to another stable and regular hopping cycle. As soon as the impact is detected, the mode controller takes over and quickly controls the springs according to the planned trajectory. If the leg inertia cannot be neglected, a retraction strategy can help to impact the ground at the matching velocity, a solution that will be explored in future works.

V. Conclusion

For the first time, a locomotion algorithm based on the excitation and stabilization of nonlinear modes was presented and validated extensively with experiments. The experimental results demonstrate that provided an appropriate method to connect the modes during the locomotion phases, the system trajectories evolve naturally along the desired eigenmanifold for different energies. The proposed control architecture fully exploits the natural oscillations of the system during the stance phase, allowing to control the system at different speeds in an efficient way. No tracking or feedback cancellations for template matching are required, not even gravity compensation. Future work will focus on extending these design principles to multi-legged floating base robots, exploiting modes during the flight phase of a leg, and comparing the efficiency with other locomotion approaches.

References

[1] A. Albu-Schaeffer and C. Della Santina, "A review on nonlinear modes in conservative mechanical systems," *Annual Reviews in Control*, 2020.

[2] T. J. Roberts and E. Azizi, "Flexible mechanisms: the diverse roles of biological springs in vertebrate movement," *Journal of Experimental Biology*, vol. 214, no. 3, pp. 353–361, 2011.

[3] C. Della Santina, M. G. Catalano, and A. Bicchi, "Soft robots," *Berlin, Heidelberg: Springer*, 2020.

[4] L. Scalera, I. Palomba, E. Wehrle, A. Gasparetto, and R. Vidoni, "Natural motion for energy saving in robotic and mechatronic systems," *Applied Sciences*, vol. 9, no. 17, 2019.

[5] J. W. Grizzle, C. Chevallereau, R. W. Sinnet, and A. D. Ames, "Models, feedback control, and open problems of 3d bipedal robotic walking," *Automatica*, vol. 50, no. 8, pp. 1955–1988, 2014.

[6] M. Calisti, G. Picardi, and C. Laschi, "Fundamentals of soft robot locomotion," *Journal of The Royal Society Interface*, vol. 14, no. 130, p. 20170101, 2017.

[7] N. Kashiri, A. Abate, S. J. Abram, A. Albu-Schaffer, P. J. Clary, M. Daley, S. Faraji, R. Furnemont, M. Garabini, H. Geyer, A. M. Grabowski, J. Hurst, J. Malzahn, G. Mathijssen, D. Remy, W. Roozing, M. Shahbazi, S. N. Simha, J.-B. Song, N. Smit-Anseeuw, S. Stramigioli, B. Vanderborght, Y. Yesilevskiy, and N. Tsagarakis, "An overview on principles for energy efficient robot locomotion," *Frontiers in Robotics and AI*, vol. 5, p. 129, 2018.

[8] W. J. Schwind, *Spring loaded inverted pendulum running: A plant model*. University of Michigan, 1998.

[9] H. Geyer, A. Seyfarth, and R. Blickhan, "Compliant leg behaviour explains basic dynamics of walking and running," *Proceedings of the Royal Society B: Biological Sciences*, vol. 273, no. 1603, pp. 2861–2867, 2006.

[10] C. Hubicki, J. Grimes, M. Jones, D. Renjewski, A. Spröwitz, A. Abate, and J. Hurst, "Atrias: Design and validation of a tether-free 3d-capable spring-mass bipedal robot," *The International Journal of Robotics Research*, vol. 35, no. 12, pp. 1497–1521, 2016.

[11] Y. Gong, R. Hartley, X. Da, A. Hereid, O. Harib, J.-K. Huang, and J. Grizzle, "Feedback control of a cassie bipedal robot: Walking, standing, and riding a segway," in *2019 American Control Conference (ACC)*. IEEE, 2019, pp. 4559–4566.

[12] R. M. Ghigliazza, R. Altendorfer, P. Holmes, and D. Koditschek, "A simply stabilized running model," *SIAM review*, vol. 47, no. 3, pp. 519–549, 2005.

[13] K. Green, R. L. Hatton, and J. Hurst, "Planning for the unexpected: Explicitly optimizing motions for ground uncertainty in running," in *2020 IEEE International Conference on Robotics and Automation (ICRA)*. IEEE, 2020, pp. 1445–1451.

[14] X. Xiong and A. Ames, "Slip walking over rough terrain via h-lip stepping and backstepping-barrier function inspired quadratic program," *IEEE Robotics and Automation Letters*, vol. 6, no. 2, pp. 2122–2129, 2021.

[15] S. H. Collins, M. Wisse, and A. Ruina, "A three-dimensional passive-dynamic walking robot with two legs and knees," *The International Journal of Robotics Research*, vol. 20, no. 7, pp. 607–615, 2001.

[16] S. Collins, A. Ruina, R. Tedrake, and M. Wisse, "Efficient bipedal robots based on passive-dynamic walkers," *Science*, vol. 307, no. 5712, pp. 1082–1085, 2005.

[17] C. D. Remy, K. Buffinton, and R. Siegwart, "Stability analysis of passive dynamic walking of quadrupeds," *The International Journal of Robotics Research*, vol. 29, no. 9, pp. 1173–1185, 2010.

[18] I. Poulakakis and J. W. Grizzle, "The spring loaded inverted pendulum as the hybrid zero dynamics of an asymmetric hopper," *IEEE Transactions on Automatic Control*, vol. 54, no. 8, pp. 1779–1793, 2009.

[19] M. Hutter, C. D. Remy, M. A. Höpflinger, and R. Siegwart, "Slip running with an articulated robotic leg," in *Intelligent Robots and Systems (IROS), 2010 IEEE/RSJ International Conference on*. IEEE, 2010, pp. 4934–4939.

[20] M. Shahbazi, R. Babuška, and G. A. Lopes, "Unified modeling and control of walking and running on the spring-loaded inverted pendulum," *IEEE Transactions on Robotics*, vol. 32, no. 5, pp. 1178–1195, 2016.

[21] M. A. Sharbafi, M. J. Yazdanpanah, M. N. Ahmadabadi, and A. Seyfarth, "Parallel compliance design for increasing robustness and efficiency in legged locomotion—proof of concept," *IEEE/ASME Transactions on Mechatronics*, vol. 24, no. 4, pp. 1541–1552, 2019.

[22] G. Garofalo and C. Ott, "Passive energy-based control via energy tanks and release valve for limit cycle and compliance control," *IFAC-PapersOnLine*, vol. 51, no. 22, pp. 73–78, 2018.

[23] B. Yi *et al.*, "Orbital stabilization of nonlinear systems via mexican sombrero energy shaping and pumping-and-damping injection," *Automatica*, vol. 112, p. 108661, 2020.

[24] C. F. Sætre, A. Shiriaev, L. Freidovich, S. V. Gusev, and L. Fridman, "Robust orbital stabilization: A floquet theory-based approach," *arXiv preprint arXiv:2011.13674*, 2020.

[25] A. F. Vakakis, L. I. Manevitch, Y. V. Mikhlin, V. N. Pilipchuk, and A. A. Zevin, *Normal modes and localization in nonlinear systems*. Springer, 2001.

[26] Z. Gan, Y. Yesilevskiy, P. Zaytsev, and C. D. Remy, "All common bipedal gaits emerge from a single passive model," *Journal of The Royal Society Interface*, vol. 15, no. 146, p. 20180455, 2018.

[27] C. Della Santina and A. Albu-Schaeffer, "Exciting efficient oscillations in nonlinear mechanical systems through eigenmanifold stabilization," *IEEE Control Systems Letters*, 2020.

[28] C. D. Santina, D. Calzolari, A. M. Giordano, and A. Albu-Schäffer, "Actuating eigenmanifolds of conservative mechanical systems via bounded or impulsive control actions," *IEEE Robotics and Automation Letters*, vol. 6, no. 2, pp. 2783–2790, 2021.

[29] L. B. Bonacchi, M. A. Roa, A. Sesselmann, F. Loeffl, A. Albu-Schaffer, and C. Della Santina, "Efficient and goal-directed oscillations in articulated soft robots: the point-to-point case," *IEEE Robotics and Automation Letters*, 2021.

[30] D. Lakatos, K. Ploeger, F. Loeffl, D. Seidel, F. Schmidt, T. Gumpert, F. John, T. Bertram, and A. Albu-Schäffer, "Dynamic locomotion gaits of a compliantly actuated quadruped with slip-like articulated legs embodied in the mechanical design," *IEEE Robotics and Automation Letters*, vol. 3, no. 4, pp. 3908–3915, 2018.

[31] C. Della Santina *et al.*, "Using nonlinear normal modes for execution of efficient cyclic motions in articulated soft robots," *International Symposium on Experimental Robotics*, 2020.

[32] A. Sesselmann, F. Loeffl, C. Della Santina, M. A. Roa, and A. Albu-Schäffer, "Embedding a nonlinear strict oscillatory mode into a segmented leg," in *2021 IEEE/RSJ International Conference on Intelligent Robots and Systems (IROS)*. IEEE, 2021.